

# On-line energy discrimination at DAQ front-end level on pixelated TOF-PET systems

Carlos Zorraquino<sup>a,b,\*</sup>, Luis Ferramacho<sup>c</sup>, Ricardo Bugalho<sup>c</sup>, Milan Zvolsky<sup>d</sup>, Agostino Di Francesco<sup>e</sup>, Carlos Leong<sup>c</sup>, Tahereh Niknejad<sup>e</sup>, Jose C. Silva<sup>e,c</sup>, Rui Silva<sup>e</sup>, Miguel Silveira<sup>c</sup>, Stefaan Tavernier<sup>c,f</sup>, Pedro Guerra<sup>a,b</sup>, Joao Varela<sup>e,c</sup>, Andres Santos<sup>a,b</sup>

<sup>a</sup>Biomedical Image Technologies Lab, Universidad Politécnica de Madrid, Av. Complutense 30, 28040 Madrid, Spain  
<sup>b</sup>CIBER-BBN - Centro de Investigación Biomédica en Red en Bioingeniería, Biomateriales y Nanomedicina, Av. Monforte de Lemos, 3-5. Pabellón 11. Planta 0 28029 Madrid

<sup>c</sup>PETsys Electronics, Taguspark, Edificio Tecnología I, 26, 2740-122 Oeiras, Portugal

<sup>d</sup>Institute of Medical Engineering, University of Lübeck, Lübeck, Germany

<sup>e</sup>LIP - Laboratório de Instrumentação e Física Experimental de Partículas, Av. Elias Garcia 14-1, 1000-149 Lisboa, Portugal

<sup>f</sup>Vrije Universiteit Brussel, Brussel, Belgium

---

## Abstract

Pixelated PET systems produce higher count rates than traditional block detectors as they integrate several detecting channels per detector module. An increased data flow from the detectors poses higher needs on the bandwidth requirements. We aim to optimize the bandwidth usage efficiency by filtering on the fly the detected events for non valid energies. PET systems with a SiPM-ASIC readout scheme are being extensively used to get enhanced images on Time-Of-Flight PET scanners. These kind of digital readout systems are specially interesting for the application of on-line processing techniques given the ease of access to each detected event digital information. This study pursues the analysis of on-line processing techniques on the DAQ front-end level (on-detector electronics) for pixelated PET systems with SiPM-ASIC readout. In particular, we worked with a tunable on-line energy discriminating stage. For the optimization of its hardwired internal limits we analyzed the system energy space. We explored different solutions dependent or not on the system's energy calibration. Results obtained through the different filter versions confirm the minimal resources consumption of such processing techniques implemented at DAQ front-end level. Our experiences showed how the filtering process reduces the bandwidth needs by excluding all non-valid energy events from the data stream and thus improving the system sensitivity under saturation conditions. Additionally, these experiments highlight how setting proper energy limits we ensure the preservation of the system performance, which maintains its original energy and time resolution. Under the light of these findings, we see a great potential on the application of on-line processing techniques for Time-Of-Flight PET at the DAQ front-end level (on-detector electronics) and so we envisaged more complex processing methods.

*Keywords:* PET, TOF-PET, Pixelated PET, SiPM, ASIC, DAQ, Digital readout, On-line processing

---

## 1. Introduction

State of the Art in Positron Emission Tomography (PET) scanners shows a tendency towards pixelated detectors opposed to monolithic ones. Pixelated systems have the potential to achieve better

spatial resolution than traditional monolithic detectors because the physical size of the detector element usually plays the dominant role in determining resolution[1]. In return, the use of highly pixelated scanners integrating thousands of detecting channels implies a higher degree of complexity on the system. The higher the degree of pixelation in the detector the more readout channels are required, thus increasing the cost and complexity of the data acquisition (DAQ) [2]. On pixelated systems the DAQ needs to handle higher detector out-

---

\*Corresponding author. Tel.: +34 915495700 ext. 4234.  
 Address: Esc. Ingen. Telecomunic. Avd.Complutense n 30-  
 Desp.C-203.1,28040- MADRID

*Email address:* carlos.zorraquino@upm.es (Carlos Zorraquino)

put data rates and an uncontrolled aggregated data flow from thousands of detecting channels could saturate the system. Traditionally, the workstation collecting all the events produced by the system performs an off-line event energy discrimination. This solution reduces the data processing computational costs cutting down the volume of data to analyze. Nevertheless, applying this technique on a highly pixelated and high count rate system does not ease the congestion issue. On these cases, the volume of data transferred from the detector electronics to the acquisition workstation tends to saturate the link between detector and data collector. Applying no particular policy to discriminate and discard events, the system dumps under saturation any event regardless of the information it contains, which results in a decrement of the system sensitivity. New on-line techniques are appearing on literature to cope with this situation. On-line energy discrimination, applied for event rejection when events' energy lays outside the valid PET energy window, is one of these techniques. On-line discriminating techniques can reduce the volume of data transferred without negative implications in the system performance [3, 4, 5, 6].

Given its system characteristics, the EndoTOFPET-US scanner [7, 8] can take advantage from the application of these on-line discriminating procedures. The EndoTOFPET-US is an asymmetric PET scanner with a main detector containing 4096 detecting channels composed of a Lutetium-Yttrium Oxyorthosilicate (LYSO) crystal pixel coupled to a Silicon Photo-Multiplier (SiPM) channel. Simulations anticipate that this 4K channels detector produces a count rate of 40 MHz [9], while real acquisitions show that the practical bandwidth (BW) limit on the system goes down to 25 MHz. Given the small size of the opposite detector, which produces no more than 200 kHz, when the system works in coincidence mode, the data rate will be below the saturation point. However, when operating the system in singles mode for detectors calibration, the bigger detector will saturate the system. Experiments with this equipment show how this 40 MHz data stream contains not only valid gamma events but a big proportion of low energy events (noise events) as well. The DAQ could drop these events with no detriment on the resulting system sensitivity because their energy is too low. Hence, the DAQ of this system [10, 11] would benefit from the on-line discrimination of events. The use of the

filter would optimize the usage of the available BW limiting the transmission to the useful data. Thus we propose an on-line discriminating solution to be implemented on the on-detector electronics, which aims to control the data volume produced by each detector module while minimizing its impact on system sensitivity and performance. Such on-detector and on the fly discriminating process would be greatly useful for highly pixelated PET scanners like the EndoTOFPET-US. It would improve detector Signal to Noise Ratio (SNR) reducing the system BW requirements.

The EndoTOFPET-US scanner implements one of the most recent techniques for PET detectors readout: SiPMs read by Application Specific Integrated Circuits (ASIC). PET detectors read by ASICs are specially adequate for the application of these on-line filtering techniques given the accessibility of the gamma event digital information. ASICs process and digitize the electrical pulse produced by the SiPM upon a gamma ray interaction on the detector crystals on the on-detector electronics. Here the Field Programmable Gate Array (FPGA) of the on-detector DAQ front-end segment retrieves the ASICs digital data. Thus making simple the gamma events energy discrimination at detector level for the DAQ module reading the gamma events' information extracted by the ASICs.

The initial hypothesis motivating this work sustains that on-line energy discrimination at detector level is an effective and lightweight solution for SiPM-ASIC PET systems to cope with the BW limitation issue present in most highly pixelated PET scanners. To prove it correct, our research first needs to confirm the potential system benefit through the study on a reference system of the resulting energy distribution of the received events. Then, to verify the effectiveness of the solution, our experiments require to study the data reduction obtained through on-line energy discrimination while analyzing the possible impact on the resulting system performance. Ultimately, to establish the discriminating module implementation cost, our investigation needs to evaluate its resources consumption.

## 2. Methods

This section describes the system considerations to take into during the filter design. It covers the implementation details of the different versions explored for the on-line energy discriminating module

and covers as well the equipment and experiments used to analyze these solutions.

### 2.1. SiPM-ASIC considerations for energy discrimination

The TOFPET ASIC [12], present on the EndoTOFPET-US main detector, uses the time-over-threshold (TOT) technique to compute the energy of the gamma events. For every detected SiPM pulse the ASIC encapsulates the information of the gamma event in a digital packet. This information includes two time stamps used to calculate the TOT: the one associated with the instant when the rising edge of the SiPM pulse surpassed the lower threshold set by the ASIC (T\_stamp) and the one associated with the instant when its falling edge falls behind the upper threshold (E\_stamp). The scheme shown in Figure 1 illustrates the thresholds positioning and the resulting time stamps when applied to SiPM pulses.

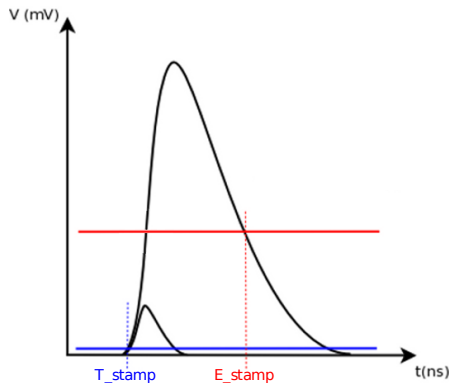


Figure 1: Dual-threshold scheme for TOT computation on a SiPM pulse: a low-threshold trigger tags T\_stamp, providing also the first time stamp for the TOT calculation. The SiPM pulse falling edge crossing the higher threshold discriminator sets E\_stamp, providing the second time stamp from which the coarse TOT can be derived.

Each of the two stamps contains two time components: coarse and fine time measurement. The coarse component has a 6.25 ns time binning and the fine one 50ps. When we use the fine time information to compute the TOT, we get a higher accuracy in the measure of the event’s energy than using just the coarse time information. However, we considered that the precision given by the coarse time information is enough for a first level on-line energy discrimination. For that reason, the filter implementations analyzed in this study ignore the fine time information and perform

energy discrimination based solely on the coarse time information simplifying the on-line discrimination modules. In practice, the on-line energy filter obtains each event’s TOT subtracting the event coarse time stamp component associated to T\_stamp (T\_coarse), to its coarse time stamp component associated to E\_stamp (E\_coarse). Equation (1) defines the general expression to compute the event coarse TOT value. During on-line event discrimination this coarse TOT value is compared against the defined energy window limits for the decision making.

$$\begin{aligned} event\_coarse\_TOT &= \\ &= event\_E\_coarse - event\_T\_coarse \end{aligned} \quad (1)$$

Since each SiPM pixel and ASIC channel of the system don’t have exactly the same performance, the response of the full system is non-uniform. The solution to this problem lays in the calibration process [11]. For each system channel, an energy calibration procedure obtains a table mapping the measured TOT and the corresponding gamma event energy in keV units. The data processing software uses this information to get the actual energy measurement for each gamma event. Regarding firmware implementation of the filter contained in the front-end electronics FPGAs, we decided to start by designing an uncalibrated version of the filter followed by its calibrated counterpart. The uncalibrated implementation ignores the energy calibration information setting the same TOT thresholds, which define the energy acceptance window, for all the channels. Whereas the calibrated version reads the energy calibration file to set channel specific energy thresholds to every single detector channel. This approach gave us the possibility to begin with a quick proof of concept of the filter using the simpler and faster-to-implement uncalibrated version. Once we finished the first stage of testing and tuning, we focused our efforts during the implementation of the calibrated filter version on calibration related issues.

### 2.2. Equipment

Given the status of the EndoTOFPET-US system at the time this study took place, which was pending for commissioning and calibration, we decided to test the filter performance on a similar but fully functional system, the PETsys Electronics demonstrator [13]. This PET system uses the

same readout electronics than the EndoTOFPET-US but with a different topology. The demonstrator integrates 2048 detector channels geometrically disposed on a small ring of detectors. Despite the differences between the two systems, all the influential characteristics for the energy discrimination process (such as ASICs, readout electronics, SIPMs and LYSO crystals) are the same for both scanners. Thus the conclusions obtained through the analysis of these tests on the demonstrator will be valid for the EndoTOFPET-US.

### 2.3. Detector energy spectrum study

After the first acquisition making use of the demonstrator system and thorough the study of the energy space of the acquired gamma events, we noticed that the TOFPET ASIC produces some events with wrong time stamps which lead to a coarse TOT out of the expected range. The upper picture on the coarse TOT map of Figure 2 shows the energy distribution of all the gamma events obtained on a 5 min acquisition with a Na22 point source centered inside the detector ring without any filtering. This graph exhibits the malfunctioning of 5 ASICs on the system. These are ASICs with channel IDs: 64-127, 192-255, 320-383, 1088-1151, 1472-1535; where channel IDs between 0 and 1023 belong to the first DAQ front-end module and between 1024 and 2047 to the second one. These five noisy ASICs produce a big number of events scattered over the whole energy space while the other ASICs rarely produce events out of the valid energy range. Analyzing a detailed view of the region of interest (coarse TOT between 0 and 70 CLK cycles) depicted in the lower plot of the coarse TOT map in Figure 2, we noticed that, despite being faulty ASICs, they still produce a bigger number of events in this region where their energies follow the same distribution than the one exhibited by the non faulty ASICs channels. This means that, although identified as malfunctioning ASICs, these ASICs produce valid data mixed with wrong time stamps events.

This data visualization indicates how an on-line energy filter would optimize the system BW usage. The distribution of events over their energy space anticipates that the main contribution to the non-useful data reduction would come from the rejection of the high concentration of low energy events considered as non-valid events. Additionally, the system would further reduce the output data rate by the discrimination of all the events cataloged

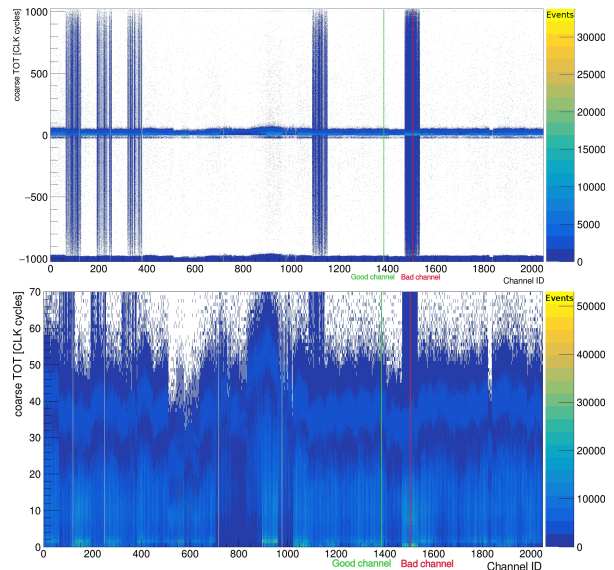


Figure 2: Coarse TOT distribution of the received ASICs events during a 5 min acquisition with a Na22 point source. Color scale indicates the number of events. The upper plot shows the complete coarse TOT span and the lower one focuses on the region of interest corresponding to the valid energy range. Both plots identify two reference channels used on our study: the “Good channel” and the “Bad channel”. These channels correspond to the system channels with the smallest and the biggest amount of noise respectively.

as events with a wrong energy information mainly given by the malfunctioning ASICs.

The full range coarse TOT map on the upper picture of Figure 2 conveys other important information too. The accumulation of events in the negative coarse TOT region close to zero indicates that for some events  $E_{\text{coarse}}$  is slightly smaller than  $T_{\text{coarse}}$ . According to the working principle of the ASIC this scenario should not arise. However, small length differences on the TOFPET ASIC electrical routes can cause deviations from the correct TOT. This discrepancy with the real difference between  $E_{\text{coarse}}$  and  $T_{\text{coarse}}$  can generate events with a negative coarse TOT close to zero for the events with the smallest energies. Furthermore, there is another abnormal concentration of events. Some events build-up in the negative coarse TOT zone close to -1024 CLK cycles, i.e.  $E_{\text{coarse}}$  close to zero and  $T_{\text{coarse}}$  close to its maximum value. The reason for it to happen is what we call the counter rollover effect. Internally the TOFPET ASIC uses a 10bits free-running counter for the time tagging of  $E_{\text{coarse}}$  and  $T_{\text{coarse}}$ . If  $T_{\text{coarse}}$  gets a value of the counter when is about to roll back to its initial

value (i.e.  $T\_coarse$  close to 1024), then  $E\_coarse$  would get a value of the counter shortly after rolling back (i.e.  $E\_coarse$  close to 0).

#### 2.4. Setting detector specific filtering rules

Correct identification and preservation of events with valid but misleading energy information is the key to preserve system sensitivity. Thus, the filter needs to exclude the events with a non-valid energy value while keeping the events which, despite containing meaningful energy information, lead to a coarse TOT computation laying outside the valid range due to the TOFPET ASIC particularities described in the energy spectrum study Section 2.3.

The acquisition SW deals with wrong energy stamps taking into account the ASIC characteristics. This SW performs a preprocessing of the received data discarding all the events which present negative energy values close to zero due to ASIC inter-path length differences. We discard these events as they are noise events with an energy close or equal to zero. Events preprocessing also takes care of the events suffering the counter rollover effect on their time tagging. For these events, the acquisition SW recomputes their resulting TOT by adding 1024 CLK cycles to the default TOT computation. Given the 10 bits size of the coarse time counter, this operation corrects the error introduced by the rollover effect obtaining the appropriate TOT of these events. The preprocessing SW uses a conservative energy limit value to differentiate events undergoing the counter rollover effect. The selection of the limit is not adapted to the detector spectrum but instead minimizes the possibility of filtering counter rollover events for most detector conditions. The filter implementation replicates these preprocessing SW rules adapting and extending them to fit the detector response analyzed in the energy spectrum study Section 2.3.

To visualize the benefit of setting detector specific filtering rules we use a visual comparison of the acquired data energy distribution for the two reference channels highlighted on Figure 2: the “Good channel” and the “Bad channel”. We selected the “Bad channel” as the system channel producing the biggest number of events, thus the noisiest system channel. Channel 1506 is the reference “Bad channel”. In opposition, the reference “Good channel” is the one producing the smallest amount of events, the less noisy channel (i.e. the one with less events with an energy outside the valid energy range). We chose channel 1390 for this purpose. To analyze

the energy distribution on a reference channel we plot the  $T\_coarse$  vs  $E\_coarse$  map of the events it produces. The time stamps distribution plots on Figure 3 show the resulting reference maps for the “Good channel” on the upper graph and for the “Bad channel” in the lower one. Setting detector specific filtering rules we intend to get rid of the events cataloged as noise. As a consequence, the newly obtained  $T\_coarse$  vs  $E\_coarse$  plots of the “Bad channel” should be alike the reference “Good channel” map after setting detector specific filtering rules.

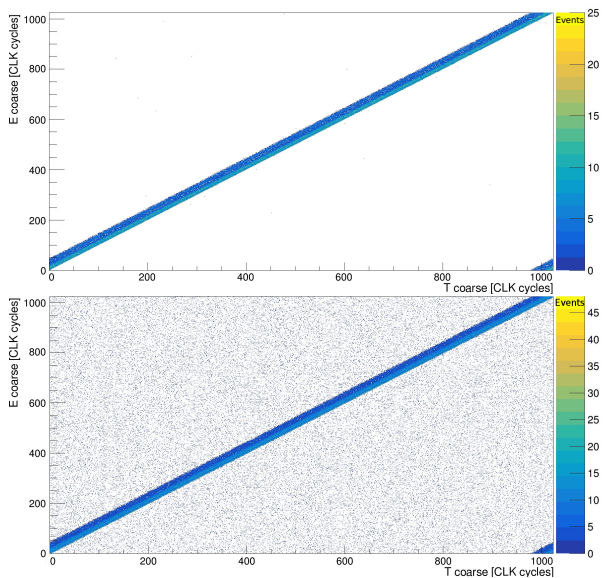


Figure 3:  $E\_coarse$  versus  $T\_coarse$  distribution of the received ASICs events expressed in ns. Color scale indicates the number of events. The produced events are the result of a 5 min acquisition placing a Na22 point source centered on the detector ring. The upper plot shows distribution for the reference “Good channel” and the lower one the distribution for the “Bad channel”

##### 2.4.1. Searching detector rollover bounds

To select the optimum coarse TOT limit value that keeps the counter rollover events while filtering out the rest of the events with a negative coarse TOT, we studied the coarse TOT distribution on the channel producing in average the highest TOT values. We designate this new reference channel as “Highest TOT channel”. Choosing this as the reference channel, we avoid setting an upper limit that would cut part of the valid events on the channels producing higher coarse TOTs than the average. The coarse TOT distribution of Figure 2 illustrates

how the ASIC with channel IDs [896:956] generates events with higher coarse TOT values. Out of these channels, 925 is the one producing the highest coarse TOTs. Thus channel 925 is the one selected as the reference “Highest TOT channel”.

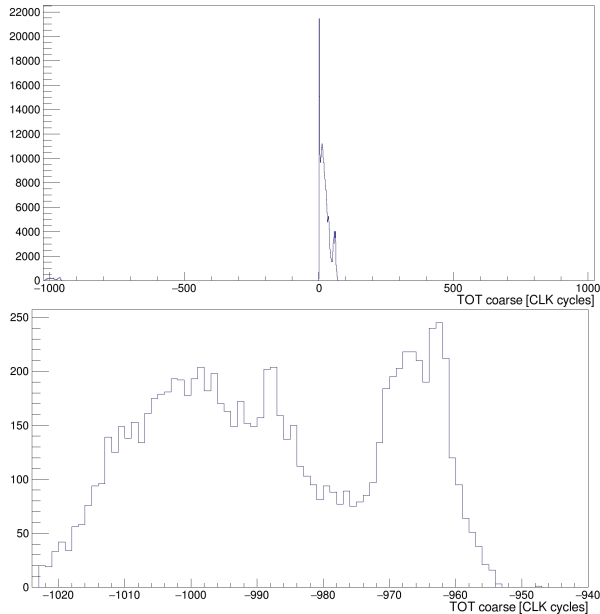


Figure 4: Coarse TOT histogram produced by the received ASIC events for the reference system channel producing the highest coarse TOT values. We express coarse TOT in CLK cycles, 6.25 ns steps. The produced events are the result of a 5 min acquisition placing a Na22 point source centered on the detector ring. The upper hand plot shows the complete coarse TOT span and the lower one focuses on the TOT region of the events suffering the counter rollover effect.

We performed five acquisitions and analyzed their coarse TOT distributions obtained for the “Highest TOT channel”. Due to the consistency of the results five acquisitions were enough to select the limits. The full span coarse TOT distribution in the upper plot of Figure 4 illustrates how, for the reference channel, most of the events lay in the region  $coarse\_TOT = [0, 80]$  CLK cycles. Events in this region do not undergo any of the TOFPET ASIC particularities. This histogram also shows a smaller concentration of events in the area  $coarse\_TOT = [-1024, -950]$ . The events with energy values within this region are the ones which suffered the counter rollover effect on their time stamping. For every acquisition, observing the distribution of events in this region of the plot, like shown in the lower coarse TOT detail of Figure 4, we extracted the maximum coarse TOT value found

on this region to define the counter rollover limit. We obtained the limit value to set on the filter by adding a three CLK cycles margin to this maximum coarse TOT value found out of the five acquisitions. As a result, we set the counter rollover coarse TOT limit to -950 CLK cycles. Adding a wider margin of CLK cycles would imply filtering less noise events but adding a smaller one could cause the filtering of meaningful counter rollover events. We chose 3 CLK cycles to balance these scenarios.

Using this information, we altered the coarse TOT computation for the TOFPET ASIC special cases obtaining the coarse TOT rollover case equation, equation (2), and the coarse TOT path length differences case equation, equation (3):

$$\begin{aligned} coarse\_TOT &= 1024 + E\_coarse - T\_coarse \\ \iff (E\_coarse - T\_coarse) &\leq -950 \end{aligned} \quad (2)$$

$$\begin{aligned} coarse\_TOT = 0 &\iff \\ -950 < (E\_coarse - T\_coarse) < 0 \end{aligned} \quad (3)$$

Using these new rules we are acting on the  $E\_coarse < T\_coarse$  region cleaning the noise events while preventing rejection of valid events undergoing the counter rollover effect. However, under the light of the observed “Bad Channel” energy distribution shown on Figure 3, we conclude that setting a filtering rule to act on the  $E\_coarse > T\_coarse$  region will further reduce the volume of data produced by a noisy ASIC channel.

#### 2.4.2. Searching detector energy upper bounds

To eliminate the noise events laying in the  $E\_coarse > T\_coarse$  region, we look for a fixed upper limit on the events acceptance window to be hardwired on the energy filter implementation along with the rollover rules expressed by the coarse TOT equations (2) and (3).

The methodology followed to select an appropriate fixed upper limit for the filter imitates the one used for the counter rollover boundary choice on Section 2.4.1. We performed five acquisitions and analyzed the energy distribution on the reference “Highest TOT channel” within the region of interest, i.e.  $coarse\_TOT = [0, 80]$ . The coarse TOT plot of Figure 5 shows an example of the kind of histograms used for the analysis. Once again, the coherence of the results between acquisitions lead us to limit the number of runs to five. For each acquisition we recorded the biggest coarse TOT value

as the upper bound of the current acquisition. To select the definitive upper bound for the filter we added a three CLK margin to the maximum of the recorded values. We selected this margin according to the same criteria as for the rollover boundary search: balance of noise reduction versus data loss.

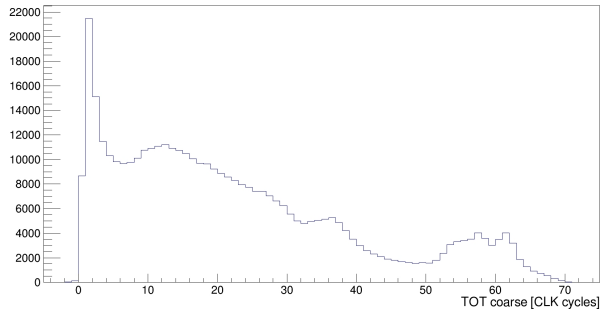


Figure 5: Coarse TOT histogram produced by the received ASIC events for the “Highest TOT channel” system’s reference channel expressed in CLK cycles, 6.25 ns. The produced events are the result of a 5 min acquisition placing a Na22 point source centered on the detector ring. The plot focuses on the valid energy range.

The on-line energy filter sets to zero the coarse TOT of the events surpassing the upper limit as shown in the new coarse TOT equation for high energies, equation (4). On the filtering stage the DAQ deletes from the data packet all events with a zero coarse TOT, including those who exceeded the upper limit, when using any low threshold setting different from zero.

$$\begin{aligned} coarse\_TOT = 0 &\iff \\ (E\_coarse - T\_coarse) &\geq 80 \end{aligned} \quad (4)$$

#### 2.4.3. Checking filtering rules effect

For a fist assessment of the noise reduction achieved through the new filtering rules we make use of the visual comparison method introduced in Section 2.4. This way we can verify the correct adaptation of the initial filtering conditions derived from the preprocessing SW to the observed system response. The E\_coarse versus T\_coarse distribution graphs of Figure 6 illustrate the effect of applying the general preprocessing SW rules on the on-line energy filter in the upper plot and the detector specific rules in the lower one.

Under the light of the data acquired making use of the on-line energy filter we can deduce that the general rules ensure preservation of events suffering the counter rollover effect while reject part of

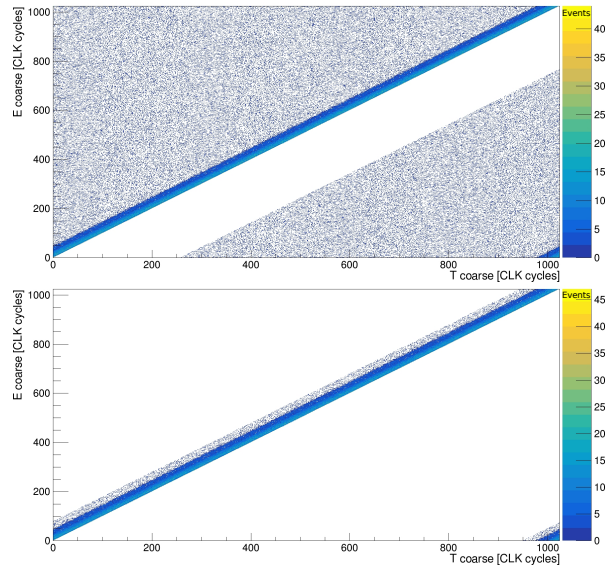


Figure 6: E\_coarse versus T\_coarse distribution of the received ASIC events produced on the reference “Bad channel” expressed in CLK cycles, 6.25 ns. Color scale indicates the number of events. The received events are the result of a 5 min acquisition placing a Na22 point source centered on the detector ring. The upper figure shows the case when the on-line discriminator implements the general filtering rules defined on the preprocessing SW. And the lower plot illustrates the detector specific rules case.

the non valid events with negative coarse TOT values. However, much more noise can be cleared out setting detector specific rules. We can observe on the lower time stamps distribution map of Figure 6 how through the new particular rules we eliminate all the noise that can be cleared out using the same unique fix margin for every channel while preserving all relevant events, even for the channels producing the highest TOT values.

#### 2.5. Uncalibrated energy filter

The complete filter implementation consists of two firmware modules plus a SW script. The Python SW script makes use of PETsys Electronics SW libraries to configure and initialize ASICs and DAQ front-end modules. Then the script sends a filter configuration command to every active DAQ front-end module setting the upper and lower thresholds for the energy acceptance window of the DAQ module’s filter. After completing system and filter configuration the script reads data through the acquisition system.

The relationship between TOT and energy is different from channel to channel. Thus, if there is

not a common TOT-energy relation for all channels, it would make no sense to express the filter thresholds in terms of energy for the uncalibrated version. Hence, thresholds set by SW are directly expressed as coarse TOT values in time units. The filter accepts only those events whose coarse TOT lays between the temporal thresholds set on the filter, independently of the actual energy that it represents. As a consequence, there would be one single pair of thresholds to set for the entire system.

The DAQ communication protocol included the definition of a set of configuration and control commands. During the configuration phase [11], the SW script sends these commands to the DAQ back-end module which will redirect them to the appropriate DAQ front-end module. For the filter implementation, we extended the configuration command space to include a new command for the filter thresholds setting. This command accepts two 10 bits numerical parameters, one for the lower threshold and one for the upper one. Even though the user specifies the filtering limits in seconds, ASICs coarse time tags are expressed in CLK cycles. Hence, the SW script converts the parameters defining the filtering limits to CLK cycles to avoid unnecessary operations on firmware, where we directly compare these values against the incoming event coarse TOT. Given the 160 MHz used to clock the system, the SW divides and rounds the thresholds given in seconds by 6.25 ns to set the thresholds directly expressed in CLK cycles. Given the 10bits length of the ASIC coarse time stamps, the 10bits thresholds parameters cover the full span of coarse TOT.

Filter firmware modules are responsible for handling its configuration commands and for the on-line filtering of incoming gamma events based on their energy. When a filter threshold-setting command arrives at a DAQ front-end module, the FPGA configuration logic block extracts the thresholds from the configuration command and passes them to the on-line energy filter stage. During the detector configuration phase the FPGA stores the thresholds on a register and it reads their values upon each gamma event arrival during the filtering stage. The on-line filtering process consists of the continuous inspection of incoming ASIC data packets. For every gamma event contained in the data packet, the filter computes the event coarse TOT either using the general case equation (1) or one of the special cases equations (2), (3) or (4). Then compares the resulting coarse TOT against the given

energy thresholds and takes the filtering decision. If the event coarse TOT lays outside the acceptance energy window the filter removes the current event from the data packet, sending to the DAQ collector module packets containing exclusively the valid gamma of events of the original data packet.

ASICs send data packets with all the detected gamma events every  $6.4 \mu s$ , i.e. every 1024 CLK cycles. Internally, the DAQ system formats the incoming ASIC data packets to deal with 64 bit words. Each 64 bit word contains either a packet header word or a single and complete gamma event and the firmware handles each word as a whole, it implements a 64 bit architecture. The firmware data reception module writes 64 bits words of the data packet on a buffering FIFO placed right before the on-line filtering stage. This is a 64 bit wide FIFO with a capacity for 1024 words. The ASIC handles 8 bits words, implementing a 8 bit architecture, thus the DAQ front-end module processes data packet 8 times faster given its 64 bit architecture. As a consequence, the DAQ front-end module compacts the back-to-back data packets produced by the ASIC and sent as a continuous data stream. Thus in the front-end FPGA the firmware processes the incoming data stream on a non-continuous burst mode. The event discriminator module reads a word from its input FIFO every time a new word is available and it has finished processing the previous one. DAQ front-end modules need one CLK cycle to process each data packet word but complete processing of a data packet by the uncalibrated energy filter takes one additional CLK cycle. Given the non continuous packet handling, where at most data packet processing takes 128 CLK cycles, the on-line energy filter module has at its disposal 896 free CLK cycles. Thus, the extra CLK cycle for a data packet processing will not incur on a problematic delay.

The DAQ on-detector front-end electronics reading the ASICs house the two firmware modules for the on-line energy filter: filter configuration module and discrimination module. While the DAQ back-end collector module electronics needs no adaptation as the filter functionality is transparent to it. Filter configuration commands use the common format of front-end configuration and control commands. Thus, DAQ collector module, who takes care of the front-end control and configuration as well, merely retransmits these commands towards the addressed front-end unit. From the point of view of data discrimination, the filter simply re-



moves events which are not in compliance with the energy rules without modifying the data packet format. As a result, the DAQ collector module needs no modifications, it processes filtered data packets as if it were any regular data packet.

The filter does not alter the event information, it merely reads the event coarse time stamps to compute its coarse TOT value for internal comparison against the energy window limits. The events, whose energy meets the acceptance conditions, pass the on-line filter unmodified. Once the filter module identifies an event with a distorted energy due to one of the two ASIC special cases, it would be simple to modify the event coarse time stamps on the fly to compensate the effects of these cases. Nonetheless, we decided to leave the stamps untouched on the first filter implementation to avoid introducing any artifact.

### 2.6. Calibrated energy filter

Given the differences in the performances of the detector channels, the system requires a calibration process to homogenize the response of the 2048 channels. This calibration process includes the energy calibration which relates TOT and its equivalent energy for every system channel. The calibrated filter version exploits the energy calibration information to set independent filter thresholds adjusted for every particular channel according to their response. As a consequence, we define the calibrated filter thresholds as real energy values expressed in electron-volts [eV]. We will need to translate these values using the energy calibration table to extract the equivalent TOT thresholds of each channel.

SiPM pulses TOT measurement is strongly non-linear [14] and we cannot model the TOT-energy relationship analytically. Thus, the calibration process obtains this relation experimentally by measuring the resulting TOT from gamma photon sources with photo-peaks of known energy. Experimental data shows an exponential TOT-energy relation, being able to fit most of the system channels with exponential functions. A conversion table is created during calibration to define each channel exponential function fit. This table relates TOT and energy for each channel and for a subrange within the expected energy range. This ranges goes from  $TOT = 0$  up to  $TOT = 499.5ns$  on 0.5 ns steps. According to experimental results  $TOT = 499.5ns$  corresponds to a value around 100MeV for most of the channels. This value above our energy range

of interest, i.e. around 511 keV, introduces a margin for the ASICs channels producing the highest TOTs.

We modified the filter SW script for the calibrated version to configure independent energy thresholds for every system channel after loading the main ASICs and front-end boards configuration parameters. For the filter configuration, we pass two parameters to the script specifying the lower and upper thresholds expressed as an energy value in keV. These thresholds define the filter energy cuts or acceptance window. For each system channel the script reads the TOT-energy conversion table searching for the closest energy values to the given filter thresholds and gets the equivalent TOT values. In some cases, the calibration points obtained for a certain channel do not permit a correct function fit with an exponential function. The configuration SW identifies those channels and configure them using the filter thresholds of the previously configured channel who presented a valid function fit. The script then constructs a configuration command containing the two TOT filter cuts for the channel under process. In the configuration command we express the threshold value to send as number of CLK cycles, like for the uncalibrated filter version, because the ASIC data packet uses the same units and thus we avoid extra firmware processing. The SW script repeats this procedure for each channel to configure the on-line energy filter thresholds of every system channel independently. Once the configuration SW sets all the system parameters including the filter ones, the acquisition SW reads data through the DAQ system.

Given the channel specificity of the new filter version configuration commands, the commands syntax changes to include the channel address. The calibrated filter configuration command follows this syntax:

- A header byte to identify the command type, which indicates that this is a filter threshold setting command.
- A 10 bits word containing the channel ID.
- A 10 bits word containing the lower threshold value in CLK cycles.
- A 10 bits word containing the upper threshold value in CLK cycles.

Though the system contains 2048 channels, the channel ID parameter of the configuration com-

mand contains 10 bits instead of 11 because it needs to identify the channel within the front-end module which contains 1024 channels. According to the DAQ communication protocol, DAQ back-end module encapsulates the filter configuration command using a header that already identifies the destination front-end module.

For the threshold values storage, on each front-end detector module the firmware implements a 20bits wide Look Up Table (LUT) with 1024 entries, one for each of its channels. This LUT is 20bits wide to store both the lower and upper thresholds for each channel entry. The filter configuration firmware module unpacks each command extracting its destination channel ID and thresholds. It uses the channel ID as the LUT address and writes its threshold values. During the configuration phase this module receives the 1024 configuration commands from the configuration SW script to fill the complete table of that particular front-end module.

During the acquisition phase, the on-line energy filtering stage continuously inspects the incoming ASICs data packets. The filtering module extracts from the packet individual gamma events information to apply the following processing:

1. Read the event channel ID and time stamps.
2. Compute the event coarse TOT according to the defined filtering rules.
3. Read the LUT using the event channel ID for addressing.
4. Compare the event coarse TOT against the threshold values read from the LUT.
5. Event rejection decision making.

Reading from LUT adds two CLK cycles for the processing of each gamma event to the one CLK cycle required by the uncalibrated version. The complete processing of the data packet, as for the uncalibrated filter version, takes one additional CLK cycle. Given the different architectures implemented by the ASICs and the DAQ front-end module (8b vs 64b), as explained in the uncalibrated filter Section 2.5, the filter has at its disposal 896 CLK cycles for the extra processing time that it needs. Hence, the filter can deal at most with 447 events per data packet, 70Mevents/s, causing no problematic delay. Simulations show how this kind of electronics will produce no more than 10Mevents/s per DAQ front-end module, which leads us to the conclusion that the on-line energy filter can absorb the volume of data produced by the detector modules on the fly.

The calibrated version of the filter has no special requirements on the DAQ collector module. The front-end modules FPGAs contain both the filter configuration and on-line processing firmware modules. The DAQ back-end module forwards the filter configuration commands and processes the incoming filtered data packets as it does for any other configuration command or data packet.

## 2.7. Experiments and laboratory methods

For the characterization of the on-line energy filter performance our experiments emulated a real PET acquisition scenario. A Sodium-22 (Na22) point source placed in the center of the demonstrator detector ring was radiating uniformly over the detectors surface on our experiments. Na22 sources are positron emitters in the same way as the radioactive isotopes used for PET tracers are. Once a positron annihilates with an electron, the process emits two back-to-back gamma photons with a 511 keV energy. The acquisitions in our experiments target the detection of these gamma rays as in real PET acquisitions. Having a source illuminating the detectors with the right energy, we can observe through the acquisitions with the on-line energy filter if the DAQ preserves data in the valid energy range while filtering out all the noise produced outside this range. According to the source aging, we estimate that the point source used on our experiments produces an activity of around 24  $\mu Ci$ .

Our main goal is to reduce the excess on the data volume produced by the system and thus our experiments analyze the influence of the filter on the system's output data rate. We studied the data reduction obtained through the tuning of the filter's low energy threshold for the different filter implementations. All the acquisitions are performed under the same conditions to have a common framework for the results comparison. Experiments maintain a constant acquisition time and use the same radioactive source. Preserving these two experiments conditions we ensure that the volume of data produced by the detector modules remains constant.

An efficient data reduction process preserves the resulting system sensitivity which directly affects on the system's performance. To prove the conservation of the system's performance, in our final experiment we placed the Na22 source centered in the detector ring and performed a long enough acquisition to get good statistics for the data analysis of the system's energy spectrum and CTR distribution. Specifically, using a 24  $\mu Ci$  Na22 source,

we found that 10 min acquisitions were needed to achieve enough statistics to produce smooth and contiguous histograms.

### 2.8. Statistical methods

The conclusions obtained from our tests are not based in the result of one single acquisition per experiment. To reduce the uncertainty in the results outcome, we performed several acquisitions for every experiment. From these acquisitions we extracted their average values and variabilities and used them to express our results. Given the consistency of the results we decided to limit the number of acquisitions per test to 5.

For the statistical data analysis and its visualization we used ROOT, a data analysis framework for statistical analysis and visualization. Through this framework we read the gamma events database created with each acquisition, extract the event's feature or features of interest for the experiment and visualize the data in the form of 1D or 2D histograms showing the distribution of the values obtained for the parameters under study.

## 3. Results

This section describes the results obtained making use of the two different versions of the on-line energy filter described in the methods Section 2.

### 3.1. Uncalibrated energy filter

During the definition of the filtering rules described in Section 2.4, we implemented different intermediate filter versions. Setting no thresholds on these filter versions and measuring the obtained data rate would give us the contribution of each filtering rule to the non-valid data rate reduction. To get the reference volume of data for comparison, we ran an additional set of acquisitions under the same experimental conditions but using no filter. The comparative column chart on Figure 7 illustrates the data reduction obtained through the different filtering rules. For each implementation we computed the average value of the 5 acquisitions and compared against the reference non filtering case to get the percentage of the data volume reduction. Error bars illustrate the variability of the data volume for acquisitions under these circumstances.

Setting no filter thresholds, this experiment gives us the raw contribution of each hardwired filtering rule. The comparative column chart on Figure 7

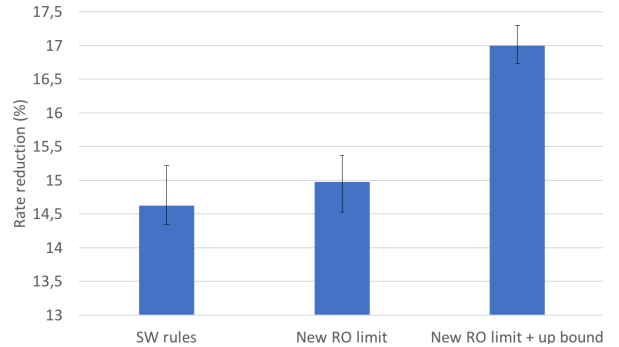


Figure 7: Rate reduction obtained with the uncalibrated filter using different filtering rules. We express the rate reduction as a percentage relative to the reference non filtering case.

shows us how setting filtering rules equivalent to the ones used by the preprocessing SW, denoted “SW rules” case on the graph, the filter produces a relevant reduction in the incoming data rate of 14.5%. This graph illustrates too the rather small contribution to data reduction attained through the setting of detector specific filtering rules. Establishing a detector specific rollover limit, “New RO limit” case, adds a 0.5% to the rate reduction obtained for the “SW rules” case, reaching a 15% rate decrease. Adding a filtering rule to reject noise events characterized by an abnormally high energy, “New RO limit + up bound” case, provides a rather small contribution but still bigger than the one given by the “New RO limit” version, getting now 17% less data than in the non filter case. To understand the meaning of these results we need to bare in mind the coarse TOT distribution shown in Figure 2. Apart from the events identified as valid events undergoing counter rollover effect present in the region  $-1024 < coarse\_TOT < -950$ , the biggest concentration of events outside the valid energy range is in the area  $0 < coarse\_TOT < -50$  which concentrates the low energy events who suffered the effect of the ASIC inter-path length differences. This concentration of non-valid events is rejected when setting SW equivalent filtering rules. Thus the “SW rules” filter implementation is the version with the biggest contribution to the rate reduction. In the other two detector specific rules implementations rate reduction is mainly given by the filtering of the non-valid events belonging to one of the five problematic ASICs identified on the system. The bigger the number of problematic ASICs present in the system, the higher the rate reduction for these

last two filter versions.

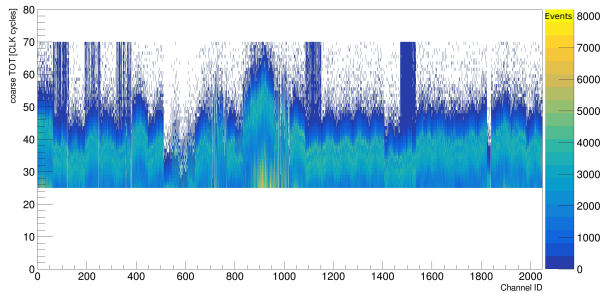


Figure 8: Coarse TOT distribution of the received ASICs events for the 2048 system channels expressed in CLK cycles, 6.25 ns. Color scale indicates the number of events. The produced events are the result of a 5 min acquisition placing a Na22 point source centered on the detector ring when using the uncalibrated filter and setting 25 and 70 CLK cycles as the filtering thresholds.

Once we found and set detector specific hard-wired filtering rules, we performed a threshold sweep searching for the best TOT thresholds to apply simultaneously on all the channels. The coarse TOT distribution on Figure 8 depicts the result of applying the threshold values found to conserve the valid events of every channel, even for those with a lower or higher coarse TOT than the average. Hence, the resulting lower threshold for the uncalibrated filter is 25 CLK cycles and 70 CLK cycles for the upper one. During the threshold sweep we recorded system's output data rate obtaining the rate evolution curve depicted in Figure 9. Through this experiment we observed how setting the optimum thresholds on the uncalibrated filter, the ones used to get the coarse TOT distribution of Figure 8, we achieve a 70% data rate reduction while preserving all the events with a valid energy.

We studied the resources consumption on the DAQ front-end module FPGA implementing the filter to judge the implementation complexity of this uncalibrated filter version. The uncalibrated filter consumes for the implementation of the filtering module plus the changes on the configuration module the following FPGA resources for our device under use, Xilinx Kintex7 XC7K160T:

- 278 slice LUTs, 0.27% of the total number of slice LUTs in the device.
- 510 slice registers, 0.25% of the total number of slice registers in the device.
- 119 slices, 0.47% of the total number of slices in the device.

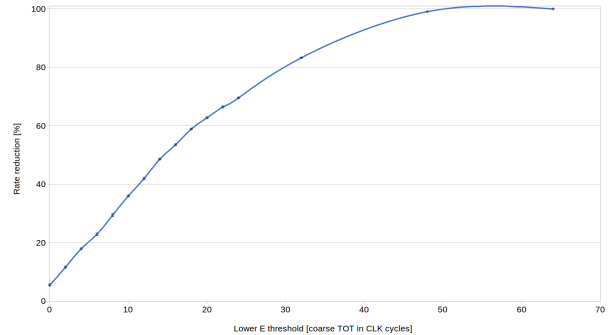


Figure 9: Rate reduction obtained through the increment of the low filter threshold when applying the uncalibrated filter. We express the rate reduction as the percentage relative to the reference non filtering case.

### 3.2. Calibrated energy filter

When we use the calibrated filter version to discriminate non-valid detected events, the resulting coarse TOT distribution of the received events presents variable energy cuts adapted to the each channel response as shown in the energy map depicted on Figure 10. One of the benefits of using channel dependent filtering thresholds is the optimum energy cuts setting that the technique provides. These channel specific thresholds led to the complete filtering of all events with an energy outside the valid energy range even for the malfunctioning ASICs. Observing the coarse TOT distribution on Figure 10 we can see how is no more possible to identify the problematic ASICs present on the system by inspection of their energy spaces. Now the filtering process is optimum, for every channel, the DAQ front-end modules only retransmit the gamma events whose energy lays within the specified energy window.

Under these conditions we performed a threshold sweep analysis to find the best energy threshold value for the current system while studying the effect on the data rate reduction. The evolution curve depicted on Figure 11 shows the progression of the data reduction as we increase the lower threshold. We can notice the higher concentration of events with low energies given the reverse exponential tendency of the curve. This result is in agreement with the energy distribution shown in the coarse TOT distribution of Figure 2. The detailed view of the region of interest in the lower plot shows how the lower energy range concentrates the biggest amount of events. Once the low threshold surpasses 150 keV the evolution on the rate reduction is not

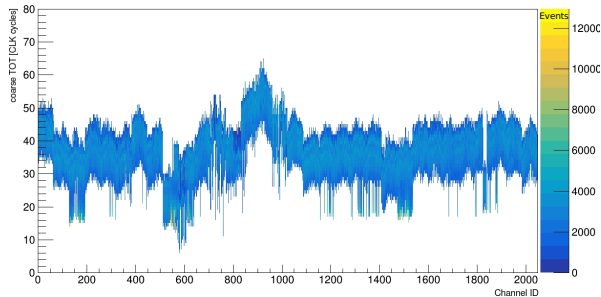


Figure 10: Coarse TOT distribution of the received ASICs events for the 2048 system channels expressed in CLK cycles, 6.25 ns. Color scale indicates the number of events. The produced events are the result of a 5 min acquisition placing a Na22 point source centered on the detector ring when the DAQ front-end modules implement the calibrated filter.

so steep. System simulations indicate how the low energy cut value which finds the best compromise between system’s sensitivity and non-valid events resuction is 225 keV for the EndoTOFPET-US system [15]. When we set a lower filter threshold equal to 225 keV we obtained a 80% data rate reduction as shown in the evolution curve depicted on Figure 11.

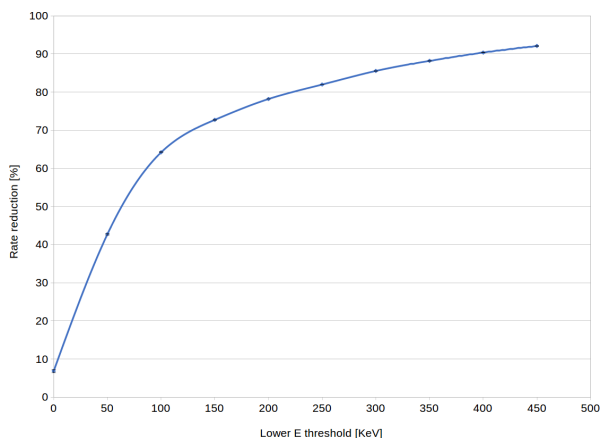


Figure 11: Rate reduction obtained through the increment of the low filter threshold when the DAQ front-end modules implement the calibrated filer. We express the rate reduction as the percentage relative to the reference non filtering case.

To analyze the complexity of the calibrated filter version we studied the resources it consumes when we implement it on the target FPGA. The FPGA utilization report shows us how there is not a significant increment in the resources demand of this version in comparison with the uncalibrated one. The calibrated filter consumes in total for the implementation of the filtering module plus the changes

on the configuration module the following FPGA resources for the device under use, Xilinx Kintex7 XC7K160T:

- 292 slice LUTs, 0.29% of the total number of slice LUTs in the device.
- 538 slice registers, 0.27% of the total number of slice registers in the device.
- 133 slices, 0.52% of the total number of slices in the device.
- 1 block RAM tile, 0.31% of the total number of block RAM tiles in the device.

There is a negligible increment on the slices resources needs in comparison with the uncalibrated filter version. The significant resources consumption difference between both filter versions comes from the implementation of the LUT to store the filtering thresholds of every channel. The implementation of this memory block consumes one FPGA block RAM tile.

Despite the indications of proper energy discrimination shown on the coarse TOT distribution of Figure 11, we need to prove that the usage of the on-line energy filter does not alter the performance of the system. To ensure that the filtering process is transparent to the system performance, we compared the resulting energy and time resolutions with the original detector resolutions. The energy spectrum comparison of Figure 12 shows the original energy spectrum of the unfiltered data in red color and the filtered case in blue. For this experiment we set a 150 keV low threshold and a 900 keV upper threshold. Observing the filtered energy spectrum on Figure 11, we can check how this thresholds are properly set because the filter lets pass only those events whose energy lies within these two values. The accuracy setting the filter thresholds is merely determined by the accuracy on the energy calibration process. For those systems whose calibration process place the optimization focus on a small energy range close to the 511 keV photo-peak, only thresholds set on a range around this value will be accurate. In this case, the further apart the thresholds are from the photo-peak, the poorer its accuracy will be. Additionally, given the fact that the relationship between coarse TOT and energy is exponential, the resolution is better for the lower energies than for the higher ones. Studying the energy spectrum comparison we can con-

clude that, when the DAQ front-end modules include the filter, it preserves its original energy resolution because the energy distribution in the photo-peak is the same for both cases, i.e. we get the same Gaussian fit curve in the 511 keV photo-peak for both energy spectrums.

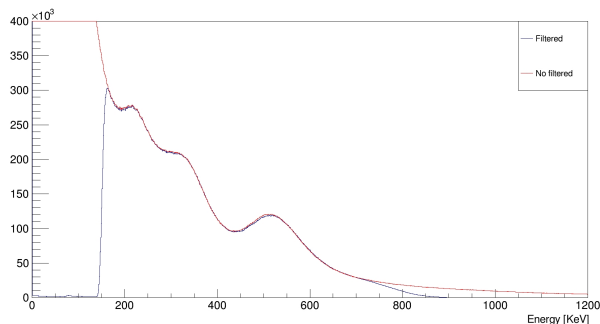


Figure 12: Energy spectrums produced by the received ASICs events. The received events are the result of a 5 min acquisition placing a Na22 point source centered on the detector when the DAQ implements no filtering at all, red curve, or when the DAQ front-end modules apply the calibrated energy filter, blue curve.

We have demonstrated how the filter does not disturb the system’s energy resolution but we still need to prove that the system maintains its temporal properties as well. For this purpose, we perform a comparison of the obtained Coincidence Time Resolution (CTR) distributions. The CTR distribution on the upper plot of Figure 13 shows the CTR distribution of the system when the DAQ implements no filtering and the lower plot displays the resulting distribution when the DAQ front-end modules apply the calibrated filter setting its lower and upper thresholds to 150 keV and 900 keV respectively. The timing results shown in Figure 13 prove the preservation of the timing properties of the system during the filtering process. For both cases, most of the recorded Lines-Of-Response present CTR values around 800 ps Full Width Half Maximum (FWHM). This is a poor time resolution for a TOF PET system and is not in agreement with the previous time resolution reported for this system [13]. The reason for having a different time resolution in this experiment is the need to deactivate the software post-processing which corrects the events time stamps off-line. Only making use of this post-processing correction the system may achieve the average CTR values of 375 ps FWHM.

The ASIC measures time of arrival of events reading the charge deposited in a capacitor. Due to a

problem on the TOFPET ASIC design, this capacitor presents a current leakage and thus the charge read from the capacitor does not corresponds to the charge associated with its time of arrival. PETsys Electronics characterized this leakage. Thus, knowing the time between consecutive events, the post-processing script can compensate the charge read from the leaking capacitor. Consequently, on systems making use of the TOFPET ASIC, the post-processing script needs the time information of the precedent event to correct the time stamp of the valid current gamma event independently of the validity of the previous event. As a result, when the DAQ filters out a non valid event, the system loses the correction information needed for the following event. Given this particularity of the TOFPET ASIC, the on-line energy filter will only preserve the time properties of the system before applying the software post-processing time correction.

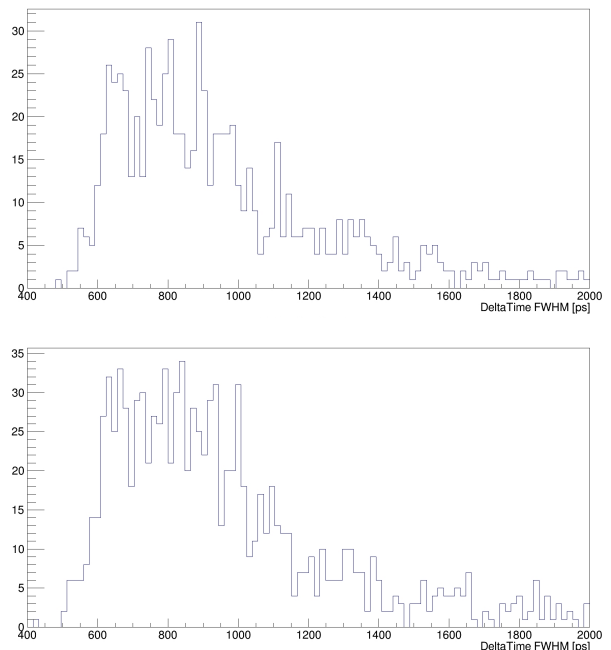


Figure 13: CTR distributions produced by the received ASICs events. The received events are the result of a 5 min acquisition placing a Na22 point source centered on the detector when the DAQ implements no filtering at all, upper graph. And when the DAQ front-end modules apply the calibrated energy filter, lower plot.

#### 4. Discussion

Under the light of the outcomes exposed in the results Section 3, we have demonstrated how the proposed implementations of the on-line energy filter are effective solutions for the reduction of the data rate in highly pixelated TOF PET systems with digital readout while preserving the system performance in terms of sensitivity and resolution (energy and time). The on-line energy filter is a lightweight solution capable of setting an energy acceptance window on demand to ease the system BW requirements.

The on-line energy discrimination technique proves to be specially useful for systems that include malfunctioning ASICs, which is common on highly pixelated systems comprising tens of these readout chips. For the exposed case of usage on the PETsys Electronics demonstrator, we have seen how these problematic ASICs on the system produce events over the whole energy range. The use of the on-line energy filter will contribute to the solution of the BW issue by filtering the events of those ASICs presenting a non valid energy value.

Experimental results demonstrate that, for the TOFPET ASIC, the biggest contribution to the data rate reduction comes from the filtering process of the events in the lowest energy range. The coarse TOT distribution on Figure 2 illustrates the higher concentration of low energy events and the coarse TOT histogram of Figure 4 confirms that there are five times more events in the lowest energy range than in the range of interest. TOFPET ASIC fails to achieve proper adjustment of its triggering scheme and thus it triggers on the reception of any detected pulse, even those with the lowest energies. Hence we can conclude that the ASIC is triggering on noise. Non being able to correct this behavior for the current readout chip, the system collects more non-valid events than valid ones. On this system, when the DAQ front-end modules implement an on-line calibrated filtering stage and setting a low threshold on 225 keV we achieve an 80% data reduction. As a consequence, we can conclude that the current system presents a poor signal to noise ratio, around 1:4, and thus it could highly beneficiate from an on-line filtering to remove the ASICs events produced from noise. In general, systems producing non valid events along with real gamma photon events find on the on-line energy filter a good solution for the efficient reduction of the system's output data rate.

Despite the proved efficiency of the filter, we have identified a couple of unexpected discrepancies on the system behavior that alter the filter outcome:

- TOFPET ASIC interdependence between consecutive events. The system needs to compensate the time information of the current event using the information of the precedent one. As a consequence, the DAQ associated to the TOFPET ASIC should not apply the on-line energy filtering to preserve the system's time resolution. Although systems readout by TOFPET ASIC chips should not apply this technique because of this ASIC particularity, we have been able to prove on this system the efficiency of the filtering process by deactivating the SW post-processing compensating the corrupted timestamps. When we disable this process, we observe how the time resolution does not vary when the DAQ implements the filter.
- High sensitivity to the energy calibration accuracy and temperature variations. By definition, the calibrated filter implementation is highly dependent on the energy calibration information. This calibration process is not straight forward in systems with thousands of channels. The curve fitting algorithm on search of the optimum TOT-energy curve does not always converge for all the system channels. For these non converging channels we have set the energy relationship found on the previous channel which exhibits a valid energy curve fit. Furthermore, given the strong exponential TOT-energy relationship, the energy calibration for the higher energy values is not as accurate as for the energies in the region of interest. Given these unexpected issues on the energy calibration process and the strong dependence of the filter on the calibration information, we found that a poor energy calibration will lead to an inaccurate positioning of the filter thresholds. Furthermore, SiPMs are highly sensitive to temperature variations [16] and changes in temperature will lead to a change on the TOT-energy relationship. Temperature variations make the present energy calibration information not valid for the new system conditions and thus the filter will fail to accurately define its filtering limits.

Comparing the similar resources consumption

and the rate reduction results obtained for the uncalibrated and the calibrated filter implementations we deduce that, in general, the calibrated filter version gives a better noise reduction on pixelated PET systems than its uncalibrated counterpart. However, given the good rate reduction results obtained using the uncalibrated filter implementation, we conclude that the uncalibrated filter version is a good solution for systems with poor or none energy calibration information.

Even-though current results deactivating the post-processing time correction are conclusive enough to prove the efficiency of the on-line filtering technique, we intend to pursue a new test using this technique on a similar system, a highly pixelated PET scanner with digital readout but this time not read by the TOFPET ASIC but by a different ASIC. One of the identified future work task is the testing of the on-line energy filter on the second version of the EndoTOFPET-US plate which makes use of the STiC ASIC[17]. The STiC ASIC does not present any interdependence between consecutive events.

Given the strong dependence of the filter with the energy calibration, which is commonly inaccurate for values not close to the 511 keV photo-peak, and the variability of the system response with temperature changes, we envisaged a new calibration independent filter implementation. This version would read all incoming data, implement a peak-finder algorithm to identify the position (TOT value) of the photo-peak for every channel and we would set the two filtering limits equally spaced on both sides of the photo-peak. This implementation will no more let the user specify the filtering energy limits in keV but instead as a margin around the photo-peak. This margin setting would enable the control of the systems output data volume while maintaining the system performance if the margin is properly set.

Another upgrade conceived for future work consists in the actual correction of the gamma events time stamps for the case of the events undergoing the counter rollover effect. The DAQ front-end modules already process the gamma events time information without modifying it. Correcting these time stamps would be a straight forward process for the DAQ and thus implementation of such process would add minimal resources needs to the filter. Making use if such on-line processing procedure would exclude the necessity of using an off-line SW preprocessing mechanism to correct the counter rollover events.

Different PET systems found in literature apply on-line data filtering techniques demonstrating its efficiency to reduce the volume of produced data minimizing the presence of non useful information [3, 4, 5, 6]. However, this is to our knowledge the first time this kind of techniques are applied on pixelated PET systems with a SiPM-ASIC readout scheme. Pixelated PET systems with a big density of digital channels are prone to present noisy channels. The more noisy channels are present on the system the less BW is available to transmit useful data. Given the ease of access to the digital information of each event on the on-detector DAQ front-end level of PET systems with SiPM-ASIC readout, we confirm that energy based event discrimination is a suitable technique to come up with the BW limitation issue present in system with a high count rate as is the case of highly pixelated PET systems.

## 5. Conclusion

Current trends in PET systems show an increasing interest on highly pixelated systems due to their capability to achieve better spatial resolution than monolithic PET systems. In turn, pixelated detectors increase the complexity of the DAQ system reading out these detectors: a high density of detecting channels produces a high count rate which could reach the system BW limit putting the system into saturation and thus losing valuable information. This work demonstrates how on-line event discrimination based on energy at the on-detector front-end level is an efficient and lightweight technique to cope with the BW limitation problem present in highly pixelated PET systems.

Furthermore, through this study we have seen how a PET system readout by the first version of the TOFPET ASIC (TOFPET ASICv1) would profit from the filtering of the non-valid energy events produced by malfunctioning ASICs. Apart from those non-useful events scattered over the energy space, this ASIC produces the highest concentration of events in the lowest energy range. In general, any SiPM-ASIC readout scheme generating events with energies out of the range of interest would reduce its BW needs making use of an on-line filtering stage discarding those events on the fly. Nonetheless, our analysis also brought into light the timing information corruption issue present on the TOFPET ASICv1 which creates an unexpected interdependence between consecutive events. Due



to this particularity of the chip, we concluded that the DAQ front-end modules should not make use this discriminating technique on systems readout by the TOFPET ASICv1. As a consequence, we plan new experiments to test the preference of the on-line energy filter on similar systems readout by other ASICs. Given the results showing the preservation of the system time and energy resolutions, even using the TOFPET ASICv1 when we disable the time correction post-processing mechanism, we conclude that on-line energy filtering is an effective technique for pixelated PET system.

Under a more global scope, this work highlights the potential of applying on-line processing techniques at the on-detector DAQ level for pixelated PET systems making use of readout ASICs. Having the digital event information in hand at the DAQ front-end modules, we could apply simple discrimination techniques as the ones here analyzed or more complex implementations as the proposed peak-finder discriminator to get a calibration independent solution.

## 6. Acknowledgment

This work, as part of PicoSEC MCNet Project, is supported by a Marie Curie Early Initial Training Network Fellowship of the European Communitys Seventh Framework Program [contract number PITN-GA-2011-289355-PicoSEC-MCNet]. And EndoTOFPETUS has received funding from the European Union 7th Framework Program, FP7/2007-2013, [Grant Agreement. No. 256984].

It does exist a potential conflict of interest given the fact that the following co-authors are employees of PETsys Electronics SA: L. Ferramacho, R. Bugalho, C. Leong, T. Niknejad, J. C. Silva, M. Silveira, S. Tavernier, J. Varela. This relationship with the company commercializing one of the devices under study does not incur in any real conflict of interest. We ensure that the information disclosed on this study is completely unbiased and objective.

## References

## References

- [1] W. W. Moses, Fundamental limits of spatial resolution in PET, *Nuclear Instruments and*

*Methods in Physics Research Section A: Accelerators, Spectrometers, Detectors and Associated Equipment* 648 (2011) S236 – S240. doi:<https://doi.org/10.1016/j.nima.2010.11.092>.

- URL <http://www.sciencedirect.com/science/article/pii/S0168900210026276>
- [2] C. Ritzer, P. Hallen, D. Schug, V. Schulz, Intercrystal Scatter Rejection for Pixelated PET Detectors, *IEEE Transactions on Radiation and Plasma Medical Sciences* 1 (2) (2017) 191–200. doi:10.1109/TNS.2017.2664921.
- [3] X. Wu, J. Zhu, M. Niu, Z. Hu, Q. Xie, P. Xiao, On-line parameter calibration for energy discrimination in trans-PET, *IEEE Nuclear Science Symposium Conference Record* (2013) 3–5doi:10.1109/NSSMIC.2013.6829181.
- [4] P. Conde, A. Iborra, A. J. González, A. Aguilar, E. Díaz-Caballero, J. J. García-Garrigos, A. González-Montoro, D. Grau-Ruiz, S. Sánchez, L. Hernández, P. Bellido, L. Moliner, J. P. Rigla, M. J. Rodríguez-Álvarez, F. Sánchez, M. Seimetz, A. Soriano, L. F. Vidal, J. M. Benlloch, Noise rejection in monolithic PET detectors, in: *2016 IEEE Nuclear Science Symposium, Medical Imaging Conference and Room-Temperature Semiconductor Detector Workshop (NSS/MIC/RTSD)*, 2016, pp. 1–5. doi:10.1109/NSSMIC.2016.8069574.
- [5] J. D. Leroux, M. A. Tétrault, D. Rouleau, C. M. Pepin, J. B. Michaud, J. Cadorette, R. Fontaine, R. Lecomte, Time Discrimination Techniques Using Artificial Neural Networks for Positron Emission Tomography, *IEEE Transactions on Nuclear Science* 56 (3) (2009) 588–595. doi:10.1109/TNS.2009.2021428.
- [6] M. A. Tétrault, A. C. Therrien, É. D. Lamy, A. Boisvert, R. Fontaine, J. F. Pratte, Dark Count Impact for First Photon Discriminators for SPAD Digital Arrays in PET, *IEEE Transactions on Nuclear Science* 62 (3) (2015) 719–726. doi:10.1109/TNS.2015.2420795.
- [7] N. Aubry, E. Auffray, F. B. Mimoun, N. Brillouet, R. Bugalho, E. Charbon, O. Charles, D. Cortinovis, P. Courday, a. Cserkaszky, C. Damon, K. Doroud, J. M. Fischer, G. Fornaro, J. M. Fournigie, B. Frisch, B. Fürst, J. Gardiazabal, K. Gadow, E. Garutti, C. Gaston, a. Gil-Ortiz, E. Guedj, T. Harion, P. Jarron, J. Kabadanian, T. Lasser, R. Laugier, P. Lecoq, D. Lombardo, S. Mandai, E. Mas, T. Meyer, O. Mundler, N. Navab, C. Ortigão, M. Paganoni, D. Perrodin, M. Pizzichemi, J. O. Prior, T. Reichl, M. Reinecke, M. Rolo, H. C. Schultz-Coulon, M. Schwaiger, W. Shen, a. Silenzi, J. C. Silva, R. Silva, I. S. Schweiger, R. Stamen, J. Traub, J. Varela, V. Veckalns, V. Vidal, J. Vishwas, T. Wendler, C. Xu, S. Ziegler, M. Zvolsky, EndoTOFPET-US: a novel multimodal tool for endoscopy and positron emission tomography, *Journal of Instrumentation* 8 (04) (2013) C04002. doi:10.1088/1748-0221/8/04/C04002. URL <http://stacks.iop.org/1748-0221/8/i=04/a=C04002>
- [8] C. Zorraquino, EndoTOFPET-US a High Resolution Endoscopic PET-US Scanner Used for Pancreatic and Prostatic Clinical Exams, in: L. M. Roa Romero (Ed.), *XIII Mediterranean Conference on Medical and Biological Engineering and Computing 2013*, Springer International Publishing, Cham, 2014, pp. 451–454.
- [9] B. Frisch, Combining endoscopic ultrasound with

- Time-Of-Flight PET: The EndoTOFPET-US Project, Nuclear Instruments and Methods in Physics Research, Section A: Accelerators, Spectrometers, Detectors and Associated Equipment 732 (2013) 577–580. doi:10.1016/j.nima.2013.05.027. URL <http://dx.doi.org/10.1016/j.nima.2013.05.027>
- [10] R. Bugalho, C. Gaston, M. D. Rolo, J. C. Silva, R. Silva, J. Varela, EndoTOFPET-US data acquisition system, Journal of Instrumentation 8 (02) (2013) C02049–C02049. doi:10.1088/1748-0221/8/02/C02049. URL <http://stacks.iop.org/1748-0221/8/i=02/a=C02049?key=crossref.53fa6832c5d9e999944e3bb8145d2cdb>
- [11] C. Zorraquino, R. Bugalho, M. Rolo, J. C. Silva, V. Vecklans, R. Silva, C. Ortigão, J. A. Neves, S. Tavernier, P. Guerra, A. Santos, J. Varela, Asymmetric Data Acquisition System for an Endoscopic PET-US Detector, IEEE Transactions on Nuclear Science 63 (1) (2016) 213–221. doi:10.1109/TNS.2016.2514600.
- [12] M. D. Rolo, R. Bugalho, F. Gonçalves, G. Mazza, A. Rivetti, J. C. Silva, R. Silva, J. Varela, TOFPET ASIC for PET applications, Journal of Instrumentation 8 (02) (2013) C02050. URL <http://stacks.iop.org/1748-0221/8/i=02/a=C02050>
- [13] T. Niknejad, S. Setayeshi, S. Tavernier, R. Bugalho, L. Ferramacho, A. D. Francesco, C. Leong, M. D. Rolo, M. Shamsirsaz, J. C. Silva, R. Silva, M. Silveira, C. Zorraquino, J. Varela, Validation of a highly integrated SiPM readout system with a TOF-PET demonstrator, Journal of Instrumentation 11 (12) (2016) P12003. URL <http://stacks.iop.org/1748-0221/11/i=12/a=P12003>
- [14] T. Orita, H. Takahashi, K. Shimazoe, T. Fujiwara, S. Boxuan, A new pulse width signal processing with delay-line and non-linear circuit (for ToT), Nuclear Instruments and Methods in Physics Research Section A: Accelerators, Spectrometers, Detectors and Associated Equipment 648 (2011) S24 – S27. doi:<https://doi.org/10.1016/j.nima.2011.01.023>. URL <http://www.sciencedirect.com/science/article/pii/S0168900211000738>
- [15] M. Zvolsky, Simulation, Image Reconstruction and SiPM Characterisation for a Novel Endoscopic Positron Emission Tomography Detector, Dissertation, Universitt Hamburg, Hamburg, dissertation, Universitt Hamburg, 2017 (2017). doi:10.3204/PUBDB-2017-13685. URL <https://bib-pubdb1.desy.de/record/398074>
- [16] M. Ramilli, Characterization of sipm: Temperature dependencies, in: 2008 IEEE Nuclear Science Symposium Conference Record, 2008, pp. 2467–2470. doi:10.1109/NSSMIC.2008.4774854.
- [17] T. Harion, K. Briggel, H. Chen, P. Fischer, A. Gil, V. Kiworra, M. Ritzert, H. C. Schultz-Coulon, W. Shen, V. Stankova, STiC a mixed mode silicon photomultiplier readout ASIC for time-of-flight applications, Journal of Instrumentation 9 (02) (2014) C02003. URL <http://stacks.iop.org/1748-0221/9/i=02/a=C02003>